Available online at www.sciencedirect.com
ScienceDirect
Journal of the European Ceramic Society 29 (2009) 1433–1442
www.elsevier.com/locate/jeurceramsoc

Influence of sputter deposition parameters on the properties of tunable barium strontium titanate thin films for microwave applications

Robert Schafranek [a,*], Andre Giere [b], Adam G. Balogh [a], Thorsten Enz [a], Yuliang Zheng [b], Patrick Scheele [b,1], Rolf Jakoby [b], Andreas Klein [a]

[a] *Darmstadt University of Technology, Institute of Materials Science, Petersenstrasse 23, D-64287 Darmstadt, Germany*
[b] *Darmstadt University of Technology, Microwave Engineering, Merckstrasse 25, D-64283 Darmstadt, Germany*

Received 4 February 2007; received in revised form 14 August 2008; accepted 24 August 2008
Available online 26 October 2008

Abstract

Barium strontium titanate (BST) thin films are studied with respect to their application as tunable dielectric at microwave frequencies. BST thin films are deposited by means of radio-frequency magnetron sputtering on platinized Si substrates. The substrate to target distance during sputter deposition is varied and the effect on structure, topology, composition and electronic properties is monitored using X-ray diffraction, atomic force microscopy, Rutherford backscattering spectrometry and X-ray photoelectron spectroscopy. These findings are related to the dielectric measurements, which are carried out at 1 MHz and in the microwave range up to 8 GHz using metal-insulator-metal structures with Pt electrodes. For further device evaluation, leakage current measurements are carried out. Changing the process parameter strongly affects the composition of the films. The results emphasize the possibility for enhancing the microwave properties by fine-tuning of the chosen process parameter.

Keywords: Dielectric properties; Functional applications; Microwave applications; Films; $BaTiO_3$ and titanates

1. Introduction

For upcoming microwave applications, capacitance tunability is one key-functionality to adjust components and systems like phase-shifters,[1,2] tunable filters[3,4] and matching networks[5,6,7] to meet future requirements, e.g. for mobile communications up to 10 GHz.[8] In comparison to already established technologies using semiconductor varactors, ferroelectric (FE) varactors offer the ability to passively tune the capacitance (C).[9] In FE varactors the tuning is achieved by applying an electrostatic field to the film to reduce the dielectric permittivity by hardening of the soft phonon mode.[10] Using a metal–insulator–metal (MIM) topology for such varactors the electrostatic tuning field can be applied by a tuning voltage U. The resulting capacitance tunability τ can be expressed by:

$$\tau(U) = \frac{C(0) - C(U)}{C(0)} \quad (1)$$

For an application of FE varactors in the microwave domain, the electric quality factor (Q-factor) and the tunability of capacitance are the most important parameters discussed in the literature.[9,11,12] These are directly related to the dielectric loss factor ($\tan\delta$) and tunability of the film. In addition, piezoelectric and acoustic properties as well as the leakage current for applied tuning voltage are also of importance for the application of FE varactors in microwave circuits. Acoustic resonances in the microwave domain excited by electrostriction leads to a reduced Q-factor of the varactor in narrow frequency bands[13] in dependence of the related piezoelectric and acoustic properties. The voltage dependent leakage current (I/V) has to be taken into account for the application of ferroelectric varactors. In addition to the related power consumption, the leakage current has also an influence on their lifetime and reliability.[14] Based on the evaluation of all these specific properties of the ferroelectric film as well as of the device, an optimal trade-off can be found for the different

* Corresponding author. Tel.: +49 6151 166354; fax: +49 6151 166308.
E-mail addresses: rschafranek@surface.tu-darmstadt.de (R. Schafranek), giere@hf.tu-darmstadt.de (A. Giere).
[1] Now at: EPCOS AG, Munich, Germany.

0955-2219/$ – see front matter © 2008 Elsevier Ltd. All rights reserved.
doi:10.1016/j.jeurceramsoc.2008.08.034

possible microwave applications to build high performance components.

For microwave applications below 10 GHz the most promising material for passive tunable components is $Ba_xSr_{1-x}Ti_{1+y}O_{3+z}$ (BST).[15,9] For this study BST with $x = 0.6$ as target material was used, which shows a phase transition between the ferro- and paraelectric phase at $T_C \approx -2\,^\circ$ C in bulk ceramics.[16] The deposition of the BST thin films is done by radio-frequency (RF) magnetron sputtering. This versatile method allows the control of the thin film properties as composition, morphology and structure. The dielectric properties of the BST thin film varactors[17,18,19] are affected by the deposition parameters as target composition, sputter power, sputter pressure and gas atmosphere as well as target to substrate distance and substrate temperature.

Depositing stoichiometric films ($y = 0$) by sputtering from ternary oxides and their mixtures can be challenging as shown for strontium titanate (STO)[17,20,21] and BST.[18] Typically an excess of Ti is observed in these oxide films which could be counterbalanced by using SrO enriched targets and by increasing the sputter pressure. Yamamichi et al. assigned the Ti excess to an amorphous TiO_{2-x} phase. Stemmer et al. have found in chemical vapor deposited BST thin films a partial accommodation of the excess Ti in the grain interior as well as in the grain boundaries by high spatial resolution electron energy loss spectroscopy. In addition, an amorphous TiO_{2-x} phase was found between the grains for high Ti excess ($y = 0.15$).[22] The cause for the excess Ti appearing in the BST thin films is believed to be resputtering and/or re-evaporation.[17]

Yamamichi et al. have found a pronounced dependence of the dielectric properties of BST thin films on stoichiometry.[21] Increasing the Ti excess of a sputtered BST thin film from $y \approx 0$ to ≈ 0.33, a decrease of ε_r from ≈ 500 to ≈ 250 could be observed. The origin of this effect is still not fully understood. Stemmer et al. suggested that the lowering of the relative permittivity is linked to the distortion of the Ti–O octahedra in the BST structure either directly by point defects created through the excess titanium or indirectly as for example by strain in the BST thin film.[22]

In this study we demonstrate the effect of the substrate to target distance during sputter deposition on the BST thin film properties. The changes of the stoichiometry of the thin films are monitored by Rutherford backscattering spectrometry (RBS). Structure and morphology are studied by X-ray diffraction (XRD), atomic force microscopy (AFM) and scanning electron microscopy (SEM). We have further analyzed the dielectric properties at 1 MHz and in the lower GHz regime as well as the leakage current (*I*/*V*) characteristic. The *I*/*V* properties are brought in conjunction with the electronic properties of the BST thin film surfaces as measured with XPS.

2. Thin film deposition and characterization

2.1. Experimental setup

The BST thin film deposition was performed by RF magnetron sputtering in a custom made ultrahigh vacuum (UHV) chamber using a 2 in. diameter ceramic $Ba_{0.6}Sr_{0.4}TiO_3$ target in an on-axis geometry. BST thin films of ≈ 300 nm thickness, as verified by ultraviolet-ellipsometry, were deposited on commercially available Si(0.3 mm)(1 0 0)/SiO_2(300 nm)/TiO_2(20 nm)/Pt(150 nm) substrates from Inostek. A sputter power density of 2.5 W/cm^2, a working pressure of 5 Pa with an Ar/O_2 ratio of 99:1 and a substrate temperature of 650 $^\circ$ C were used. The substrate to target distance d was varied between 5 cm and 10 cm, leading to deposition rates between 7 nm/min and 0.85 nm/min, respectively. 400 nm thick RF sputtered Pt top electrodes were structured by lift-off lithography. After top electrode processing, a first set of dielectric and *I*/*V* measurements were conducted. Subsequently, the samples were annealed for 30 min at 600 °C in ambient air in an alumina tube furnace followed by a second set of dielectric and *I*/*V* measurements.

The structure of the thin BST films was analyzed by X-ray diffraction in Bragg Brentano geometry using a *Siemens D5000* diffractometer with Cu Kα radiation. The morphology was probed by an atomic force microscope *ThermoMicroscopes Autoprobe CP research* in contact mode. The composition of the films was analyzed by Rutherford backscattering spectrometry using 2.0 MeV $^4He^+$ ions and a backscattering angle of 171°. Rutherford backscattering allows for precise determination of the thin film stoichiometry without calibration standards required in contrast to methods like wavelength dispersive and energy dispersive X-ray spectrometries (WDS and EDS).[23] For probing the surface composition and electronic properties of the BST thin films, XPS measurements were performed using a *Physical Electronics PHI 5700* multitechnique surface analysis system. The sputtering chamber is connected to the surface analysis system via a UHV sample transfer to exclude contamination of the BST thin film surface. X-ray photoelectron spectra were recorded with monochromatic Al Kα radiation having an energy resolution of ≈ 0.4 eV, as determined from the Gaussian broadening of the Fermi edge of a sputter cleaned Ag sample.

2.2. Results and discussion

A cross-sectional high resolution scanning electron microscope (HRSEM) picture of a Si/SiO_2/TiO_2/Pt(1 1 1)/BST layer stack is shown in Fig. 1(a). The sample has been deposited at a substrate to target distance of 8.8 cm. The different layers of the thin film stack can be identified. Unfortunately, the Pt is torn apart due to its high ductility and covers the Pt/BST interface in the image. The BST film shows no morphological defects (pinholes), a homogeneous thickness and low surface roughness in accordance with the AFM measurement (see Fig. 1(b)).

The lateral grain size and root-mean-square roughness (R_{rms}) deduced from the AFM measurements of samples prepared with different substrate to target distances are presented in Table 1. The morphology of the BST thin film surface changes strongly with variation of the sputter distance. The roughness decreases monotonically from $R_{rms} = 4.5$ nm at $d = 10$ cm to $R_{rms} = 1.7$ nm at $d = 5$ cm while the lateral grain size D increases by roughly a factor of 2.

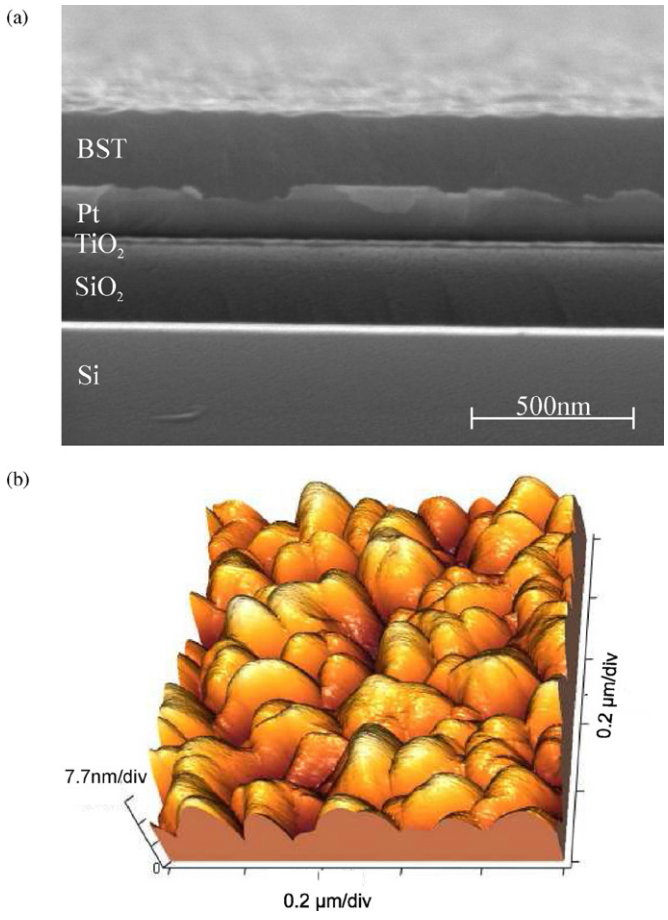

Fig. 1. (a) High resolution scanning electron microscope image of the cross-section of the Si(1 0 0)/SiO_2/TiO_2/Pt(1 1 1)/BST layer stack deposited at a target to substrate distance of 8.8 cm and (b) an atomic force microscope image of the BST thin film surface of the same sample.

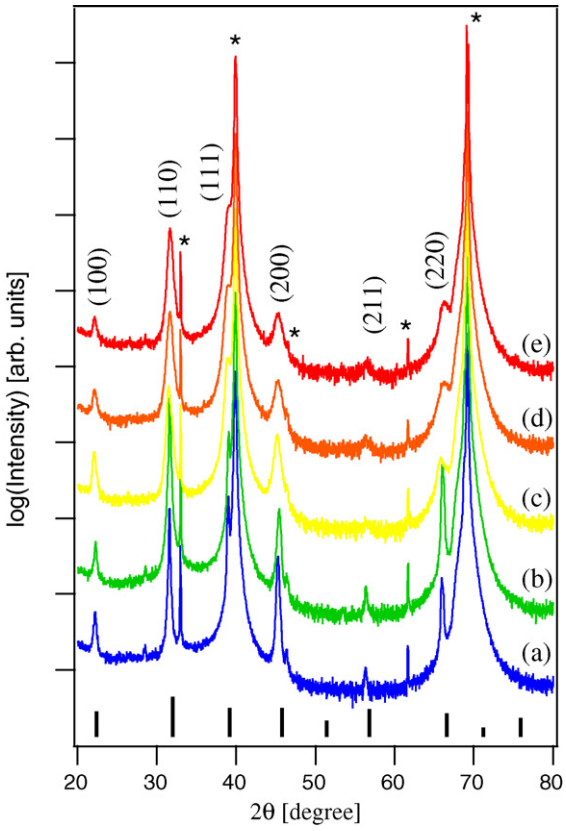

Fig. 2. X-ray diffraction patterns of the BST thin films deposited at substrate to target distances of 5 cm (a), 6.3 cm (b), 7.5 cm (c), 8.8 cm (d) and 10 cm (e) on Si(100)/SiO_2/TiO_2/Pt(111) substrates. Substrate related peaks are identified by asterisks. The intensities of powder diffraction data for BST taken from PDF 034-0411 are added for comparison. The intensity is shown in logarithmic scale.

X-ray diffraction patterns of the BST thin films are presented in Fig. 2 showing all major reflections of the cubic perovskite structure. The relative integrated intensity of the BST (1 1 1) reflection after subtraction of the nearby Pt (1 1 1) reflection is slightly stronger than expected for a BST powder sample. This indicates a weak texture of the BST film with a preferred (1 1 1) orientation being predetermined by the (1 1 1) texture of the platinized silicon substrate. The full width at half maximum (FWHM) gives an indication of the grain size normal to the surface when measured in Bragg–Brentano geometry. The FWHM is increasing significantly with larger substrate to target distance during sputter deposition, particularly for the samples deposited at $d = 8.8$ cm and $d = 10$ cm. This points to a reduction of the grain size normal to the surface plane for large substrate to target distance. This corresponds well to the decrease of the lateral grain size with increasing substrate to target distance d as measured by AFM.

Table 1
BST thin film properties in dependence on the substrate to target distance d during sputter deposition

d (cm)	D (nm)	R_{rms} (nm)	Ba/Sr	y	R (nm/min)
5	190	1.7	0.57/0.43	0.26	7
6.3	190	1.8	0.56/0.44	0.27	4.5
7.5	213	2.5	0.57/0.43	0.09	2.4
8.8	135	3.8	0.56/0.44	0.07	1.4
10	108	4.5	0.56/0.44	0.04	0.85

The lateral grain size D and the root-mean-square roughness R_{rms} are determined from AFM. The Ba/Sr ratio and the Ti excess $y = (\mathrm{Ti}/(\mathrm{Ba} + \mathrm{Sr})) - 1$ are deduced from RBS measurements. The deposition rate R is determined from film thickness as derived from ultraviolet-ellipsometry and deposition time.

A RBS spectrum of the ≈ 300 nm thick BST layer deposited at $d = 7.5$ cm on the platinized Si substrate is shown in Fig. 3. In RBS spectrometry, the different chemical elements can be separated by their different onsets, which are shifted to smaller energies for buried layers as, e.g. Pt. The composition is deduced from the integral intensities of the RBS peaks. RBS measurements of ≈ 100 nm thick BST films deposited on Si substrates were performed for comparison. The corresponding spectra shows no peak of the substrate Pt and the Ba, Sr, and Ti peaks show no overlap. The composition deduced from these films were identical to those obtained from films used for dielectric measurements.

The Ba/Sr ratio and the Ti excess $y = \mathrm{Ti}/(\mathrm{Ba} + \mathrm{Sr}) - 1$ determined from RBS are summarized in Table 1. While the Ba/Sr ratio stays rather constant at a value close to the nominal target composition, an increase of the Ti excess in the deposited BST thin films from $y = 0.04$ for $d = 10$ cm to $y = 0.26$ for

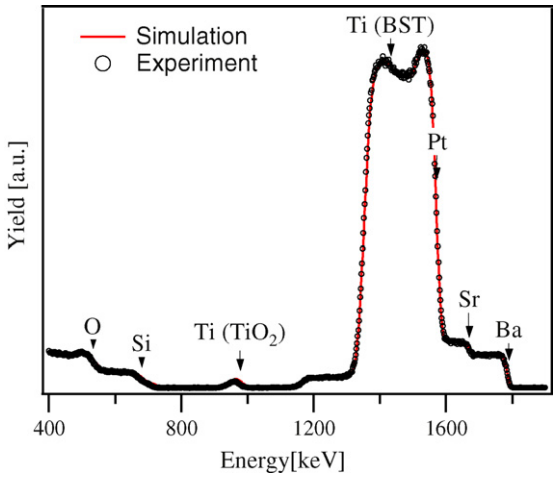

Fig. 3. Rutherford Backscattering spectrum of the BST thin film deposited at 7.5 cm sputtering distance. The simulation has been performed with the RUMP software. The edges of the respective elements are marked in the graph. For Ti the onset for the BST layer and the TiO_2 layer are marked separately.

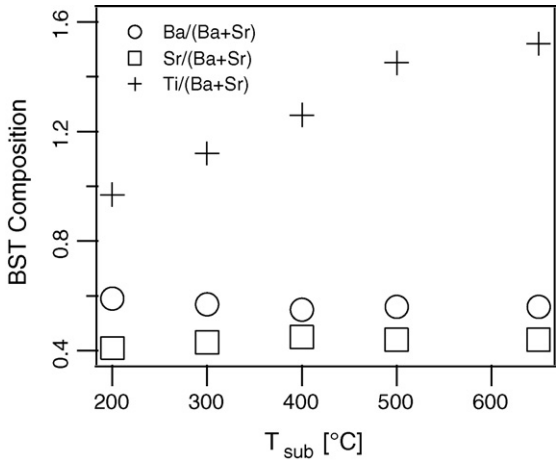

Fig. 4. Composition of the BST thin films deposited at substrate to target distance of 5 cm with varying substrate temperature as measured by XPS. The Ti excess increases with rising T_{sub} while the Ba/Sr ratio stays rather constant.

$d = 5$ cm is observed with decreasing substrate to target distance. For small Ti excess ($y < 0.15$), the Ti excess can be accommodated in the grains and grain boundaries. Amorphous TiO_{2-x} precipitations occur between the grains for larger Ti excess.[22] Such precipitations might also explain the smoother BST surfaces at smaller sputter distances (see Table 1).

Supplementary evidence for the accommodation of Ti in the grain boundaries can be deduced from the surface composition as measured by XPS. For the rather stoichiometric BST films deposited at $d = 10$, 8.8 and 7.5 cm (Ti/(Ba + Sr)) (TBS) ratios of 0.79, 0.81 and 0.9 are found while the films deposited at smaller $d = 6.3$ and 5 cm show TBS ratios of 1.39 and 1.41 (equals $y = 0.39$ and 0.41), respectively. The TBS ratios < 1 can be explained by an underestimation of the Ti-content using the sensitivity factors given by the manufacturer of the surface analytic system[24] for intensity calculation. Strontium titanate single crystals annealed for 30 min at 650 °C in 0.05 Pa oxygen show Ti/Sr ratio of ≈ 0.9. As no enrichment of SrO at the surface is expected at such low temperatures[25,26] a segregation of Ba and Sr at the BST surface can be excluded. The drastic increase in the Ti content at the BST surface as compared to the RBS-results of the BST bulk (see Table 1) for the BST thin films deposited at $d = 5$ and 6.3 cm is therefore attributed to an accumulation of Ti at the surface or grain boundaries, respectively.

The reduced roughness and the increase of the Ti excess with increased sputter distance are in accordance with the findings presented by Im et al.[18] They prepared BST thin films with similar sputter conditions using a fixed sputter distance of $d = 10$ cm and varying the total pressure during deposition. A roughness of $R_{rms} = 3.2$ nm and a Ti excess $y = 0.02$ are observed for a pressure of 7.7 Pa. Using a pressure of 2.9 Pa, a roughness of 2.1 nm and a Ti excess of $y = 0.37$ are observed. Increasing the target to substrate distance or the total pressure during sputter deposition leads to a similar decrease of the deposition rate (see Table 1 and Ref. 18). For comparison of the sputter conditions, the product of sputter pressure and distance have to be taken into account[27] explaining the similar effect of reducing sputter pressure (as done by Im et al.) and sputter distance (as done in this work) on composition and roughness.

The crystallinity of the BST thin films is improved by lowering the sputter distance as can be seen from the narrowing of the reflections in the X-ray diffractograms in Fig. 2. These results contrast the findings of Im et al. who observed a decrease in crystallinity with decreasing sputter pressure and do not find any BST-related reflexes for their films containing a Ti excess of $y = 0.37$ and 0.17. This indicates that changing the sputter pressure or the distance are not completely equivalent.

For further understanding of the formation of the Ti excess the composition of BST thin films is studied with variation of the substrate temperature T_{sub} using a substrate to target distance of 5 cm. When increasing the substrate temperature from 200 to 650 °C the TBS ratio increases from 0.97 to 1.47 while the Ba/Sr ratio is nearly independent on T_{sub} as measured with XPS. The dependence of the composition on T_{sub} is shown in Fig. 4. According to the observed dependence on substrate temperature, the increase of the Ti content is most likely explained by re-evaporation of Ba and Sr from the substrate surface during growth. Ba and Sr exhibit considerable lower evaporation enthalpies and higher vapor pressures compared to Ti and are therefore more likely to re-evaporate with increasing substrate temperature.[28] The dependence of the Ti excess on the sputter distance can then be explained by the influence of the deposition rate. Decreasing the sputter distance leads to an increase of the deposition rate while the oxygen content in the sputter gas stays constant. As the oxygen pressure is not changed, a faster deposition rate leads to an increased excess of metal atoms on the surface and consequently to an increased re-evaporation of Ba and Sr. A similar observation has been made for Al-doped ZnO films, where an increased Al content is observed with increasing substrate temperature during deposition.[29]

The binding energy (BE) of the valence band maximum (VBM) BE_{VBM} with respect to the Fermi energy (E_F) is extracted from the leading edge of the valence band measured by XPS. At the interface between the Pt bottom electrode and BST as deposit BE_{VBM}=2.2 eV is found. This height corresponds to a

Table 2
Leakage current density and dielectric behavior at 1 MHz of annealed Pt/BST/Pt capacitors

d [cm]	$\varepsilon_r(0)$	τ (15 V) [%]	Q (0)	Q (15 V)	J (−15 V) [A/cm^2]	BE_{VBM} [eV]	η (15 V)
5	213	26.2	204	131	2×10^{-2}	2.66	34.3
6.3	212	28.1	318	310	7×10^{-3}	2.65	87.1
7.5	478	65.1	47	138	2×10^{-4}	2.49	30.6
8.8	321	52.7	51	79	$< 2 \times 10^{-5}$	2.36	26.8
10	355	53.4	55	88	$< 2 \times 10^{-5}$	2.32	29.4

The untuned permittivity ($\varepsilon_r(0)$) and tunability at 15 V of the BST films as well as Q-factors of the varactors based on these films characterized at 1 MHz are shown. The leakage current density measured at −15 V and the binding energy position of the valence band maximum BE_{VBM} are added. For an evaluation the resulting material quality factor η as defined in Eq. (4) is used.

Schottky barrier for the electrons of 1.0 eV[30] taking the band gap of 3.2 eV for BST into account. For the BST thin film deposited at $d = 10$ cm a value $BE_{VBM} \approx 2.3$ eV is found at the BST surface indicating almost flatband situation as expected for an insulator with low charge carrier concentration. With smaller target to substrate distance and increasing Ti excess BE_{VBM} rises up to ≈ 2.7 eV for $d = 5$ cm. This result equals a band bending of 0.5 eV in the BST thin film indicating a rise in carrier concentration being in accordance with an increase of doping level with reduced d. An increased doping level is consistent with a rise in leakage current (see Section 3.2). The values of BE_{VBM} for the different target to substrate distances are shown in Table 2.

In XPS the difference between the binding energies of the core level lines and the valence band maximum is a characteristic attribute of a material.[31] With changing the sputtering distance and therefore the Ti excess in the BST thin films, these values show no significant change assuring no fundamental change in the deposited thin film material and reliable values for the valence band maxima. The binding energy difference between the Sr $3d_{5/2}$, Ti $2p_{3/2}$, O 1s emissions and the valence band maximum amount to 130.55 ± 0.05 eV, 455.81 ± 0.07 eV and 527.14 ± 0.06 eV, respectively. The given tolerance is deduced by the standard deviation of the corresponding binding energy differences of the measured samples.

3. Dielectric characterization at 1 MHz and *I*/*V* measurements

3.1. Experimental setup

The realized BST varactors are measured at a controlled temperature of 22 °C. To contact the varactor, Ground-Signal-Ground (GSG) probes are used as shown in the cross-section in Fig. 5(a).

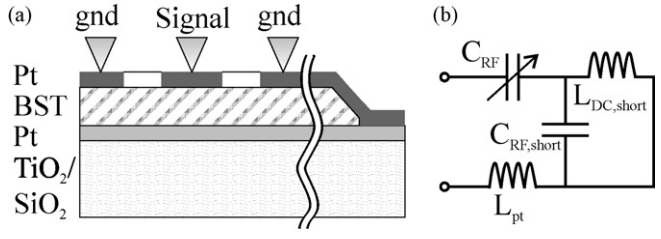

Fig. 5. (a) Cross-section of the varactors test-structure and (b) the related equivalent circuit.

The equivalent circuit of the varactor test structure is shown in Fig. 5(b). The tunable capacitor C_{RF} is formed by an octagon shaped pad connected by the signal contact of the GSG-probes. The surrounding large ground plane is represented by the capacitance $C_{RF,short}$ which acts on the microwave signal as a short circuit by $C_{RF,short} \gg C_{RF}$. This $C_{RF,short}$ is hot-wired at an edge of the substrate to be able to apply the tuning voltage only on C_{RF}. The influence of the inductance of the Pt electrodes L_{Pt} connected in serial to C_{RF} can be neglected at 1 MHz while it effects the varactor characteristics in the GHz range significantly as discussed in context with the GHz measurements (Section 4). The shown configuration allows to equate the measured capacitance C with C_{RF} at 1 MHz.

For the characterization of the FE film behaviour at 1 MHz as well as in the microwave range, we are using two different geometries to reduce measurement uncertainties due to impedance mismatch between the varactor and the optimum impedance range of the setup. The two varactor types are shown in Fig. 6(a) and (b).

By using a constant pad geometry and a relatively constant BST film thickness of $h_{BST} = 300$ nm the capacitance measured on-wafer are directly related to the BST film properties. Using simple assumption of a parallel plate capacitor for C_{RF}, the relative permittivity can be computed from the measurement:

$$\varepsilon_r = C \frac{h_{BST}}{\varepsilon_0 A_{pad}} = Cg \tag{2}$$

This assumption neglects fringing fields and other parasitics, which leads to an error in ε_r of <4% for the capacitance measured at 1 MHz computed by using the equations from Ref. 32. Using the 1 MHz suited varactor type in Fig. 6(a) the geometry factor is $g = 6.72\ pF^{-1}$ while using the varactor type in Fig. 6(b) for the GHz measurements the factor is $g = 60.5\ pF^{-1}$. The loss-factor ($\tan\delta$) of the dielectric BST film can be estimated at 1 MHz from the Q-factor of C_{RF} by

$$\tan\delta \approx \frac{1}{Q} \tag{3}$$

neglecting additional losses.[33] To compare the properties of the ferroelectric film without simplification we further use the Q-factor to illustrate the BST film loss-factor.

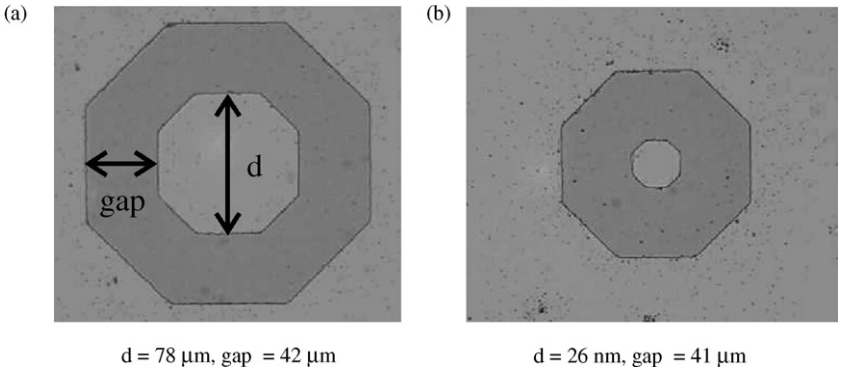

Fig. 6. Photographs of the BST thin film capacitors for (a) 1 MHz and (b) microwave measurement.

3.2. Results

After deposition of the Pt top electrodes and before the additional annealing step, we first characterize the test structures by *C/V* measurements using a *HP 4279A* unit to measure the varactor behavior at 1 MHz. The resulting capacitance tuning is shown in Fig. 7. It depicts the dependence of the sputter distance on the untuned (0 V) capacitance value, which is directly related to the relative permittivity. The capacitance is small ($C \approx 30$ pF) for sputter distances of $d = 5$ cm and 6.3 cm, maximum ($C \approx 70$ pF) for $d = 7.5$ cm and $C \approx 50$ pF for larger d. The capacitance for the maximum tuning voltage ($U = 20$ V) is $C \approx 20$ pF and does not depend on d. Consequently, the film deposited at an intermediate distance of $d = 7.5$ cm, which exhibits a moderate Ti excess of $y = 0.09$, shows the highest untuned permittivity ($\varepsilon_r(0) = 468$) as well as the highest tunability ($\tau(20\,\text{V}) = 71\%$).

At 1 MHz the measurements are made by sweeping the tuning voltage from $U = 0$ V to +20 V, to $U = -20$ V and again to +20 V within 40 s to get also an information about the hysteresis behavior of the BST thin film.

The *Q*-factor of the varactors are shown in Fig. 8(a). The BST thin films deposited at varied sputter distance show significantly different behaviour. While the samples with high Ti excess ($d =$ 5 cm and 6.3 cm) show a pronounced asymmetry of the *Q*-factor and the related dielectric loss-factor, the varactors with low Ti excess deposited at 7.5–10 cm show a symmetric behaviour with rather low *Q*-factors at 1 MHz in the untuned state. In contrast, the *Q*-factor of the varactor based on the film with the highest Ti excess ($d = 5$ cm) is above 150 for all positive tuning voltages.

To compare the effect of the subsequent annealing in oxygen at 600 °C for 30 min, the *Q*-factor of the varactors after annealing is shown in Fig. 8(b). The capacitances are almost unaffected by the annealing step and therefore still largely represented by the curves in Fig. 7. Only the hysteresis for the varactors deposited at 7.5–10 cm are less pronounced after annealing. Before annealing the maximal capacitance value is achieved at −1.3 V and decreases to −0.5 V after annealing when sweeping the tuning

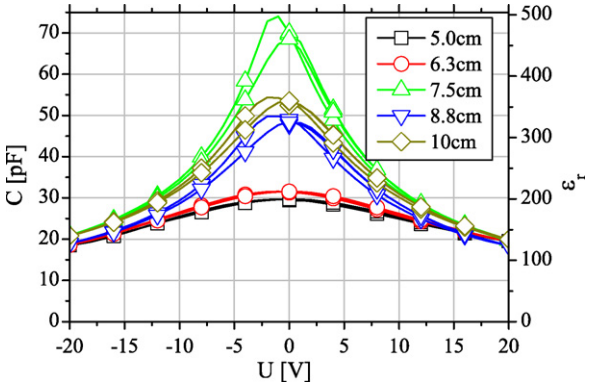

Fig. 7. Capacitance tuning of BST thin film varactors for the different sputter distances at 1 MHz before the additional annealing step. No strong change of the *C/V* curves after annealing can be observed. The to the capacitance value related relative permittivity is shown at the right axis.

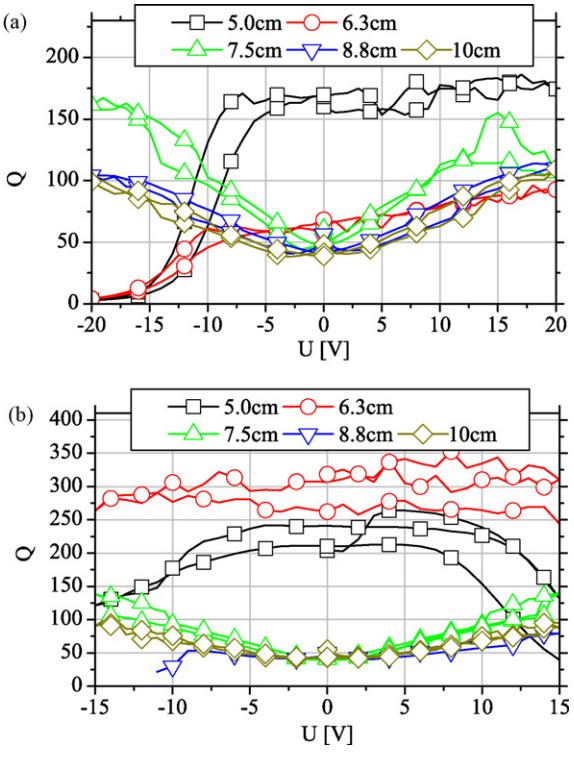

Fig. 8. *Q*-factor versus tuning voltage of BST thin film varactors for the different sputter distances at 1 MHz (a) before and (b) after the additional annealing step.

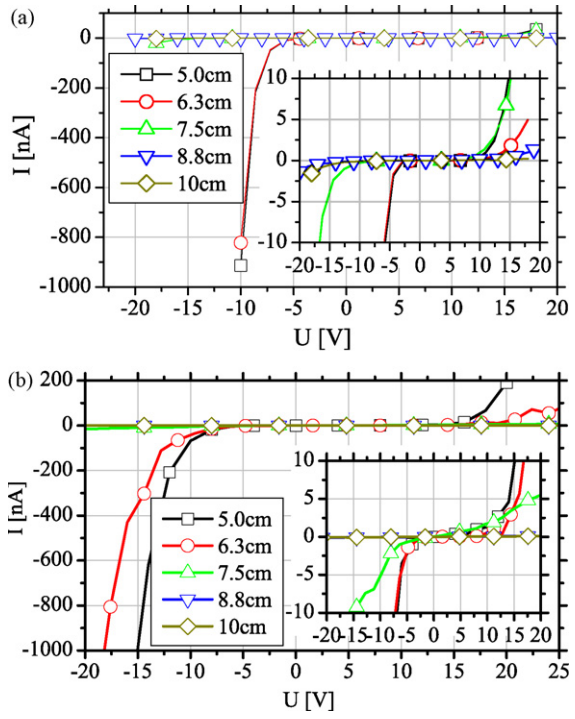

Fig. 9. Leakage current measurement (a) before and (b) after the additional annealing step for the BST varactors prepared with varied substrate to target distance during BST deposition.

voltage from $U = +20$ V to -20 V. When tuning in the reverse direction from $U = -20$ V to +20 V the capacitances maximum is at 0 V before and after annealing.

In contrast, significant changes are observed in Q-factor of the films deposited at small distances (5 cm and 6.3 cm). Their originally asymmetric dependence becomes almost symmetric. The Q-factor for the film prepared at 6.3 cm is further improved to $Q > 250$ for all tuning voltages.

To further study the impact of the annealing step on the electrical properties of the capacitors, leakage current measurements have been performed. Fig. 9(a) depicts the leakage current of the varactors up to ±20 V before annealing. The leakage current is measured with a *Keithley 2602* sourcemeter, which has an accuracy in the sub-nA range. Current densities J can be computed by $J = I/A = I/5.04 \times 10^{-5}$ cm^2. The I/V characteristic after annealing is shown in Fig. 9(b).

The measurements illustrate again the asymmetric behavior of the BST thin film capacitors with BST films deposited at 5 cm and 6.3 cm substrate-target distance with a pronounced slope of the leakage current at a bias voltage of $U < -8$ V. The leakage current of these films is reduced after the additional annealing step. The onset of strong leakage of $I < -350$ nA ($J \approx -7.0 \times 10^{-3}$ A/cm^2) is shifted after annealing to -15 V ($d = 6.3$ cm) and -12.7 V ($d = 5$ cm), respectively. The films deposited at 8.8 cm and 10 cm show leakage currents < 110 pA ($J = 2.2 \times 10^{-6}$ A/cm^2) within the tuning range of ±20 V after annealing, which is at the limitation of the used setup. Before annealing, the measured currents are within a range between 2.3 nA ($J = 4.6 \times 10^{-5}$ A/cm^2) at 8.8 cm and 1.7 nA ($J = 3.4 \times 10^{-6}$ A/cm^2) at 10 cm. This findings are comparable to the literature.[18,34]

3.3. Discussion

The relative permittivity of the BST thin films exhibits low values of $\varepsilon_r(0) \approx 210$ for thin films deposited at small substrate to target distances ($d = 5$ cm and 6.3 cm), reaches a maximum of $\varepsilon_r(0) \approx 478$ at $d = 7.5$ cm and decreases again to $\varepsilon_r(0) \approx 321$ and 355 for $d = 8.8$ cm and 10 cm, respectively. The tunability shows a corresponding behaviour: $\tau(15\,\text{V})$ increases from $\approx 27\%$ ($d = 5$ cm and 6.3 cm) to 65.1% and falls to $\approx 53\%$ ($d = 8.8$ cm and 10 cm).

The low relative permittivity and tunability of the BST thin films deposited at 5 cm and 6.3 cm can be related to their Ti excess.[21,17,35] The decreased relative permittivity and tunability of the BST thin films deposited at the largest distances of 8.8 cm and 10 cm can be attributed to their smaller grain size compared to the sample deposited at $d = 7.5$ cm as measured by AFM and XRD (see Table 1). Furthermore, thin films prepared with high sputter pressure and distance tend to have lower density and higher porosity,[36] thereby lowering the effective relative permittivity.

For the evaluation of the different performance of the prepared BST varactors, the material quality-factor η can be used to combine tunability and the minimum Q-factor $Q_{\min}$ of the varactor, where η is defined as

$$\eta = \frac{\tau}{(\tan\delta)_{\max}} \approx \tau Q_{\min} \tag{4}$$

The resulting η is shown in Table 2 for a tuning voltage of 15 V, which corresponds to a tuning field-strength in the BST film of 50 V/ μm. Table 2 also shows a short summary of the 1 MHz results and the leakage currents measured on the different annealed BST thin films.

The asymmetric Q and I/V curves for the two films exhibiting the highest Ti excess can be explained by the different contact properties at the back and front contact after Pt top electrode preparation. After Pt deposition on (clean) BST thin films, small Schottky barrier heights are found which can be increased by an annealing step in oxygen.[34,37,38,30] Using I/V measurements, Baniecki et al. have determined a Schottky barrier height for the electrons at the Pt/BST interface after Pt deposition of 0.69 eV, which is increased to 1.29 eV after oxygen annealing. The bottom contact, however, shows a high Schottky barrier directly after BST deposition on Pt explaining the asymmetry in Q-factor prior and after annealing in oxygen. This has recently been directly shown by photoelectron spectroscopy of the contact formation between BST as substrate and Pt as deposit and vice versa.[30]

The behaviour of the BST thin films with low Ti excess is not completely understood. Previous experiments with 200 μm diameter Pt top electrodes deposited on BST thin films prepared with $d = 10$ cm showed an increase of Q after oxygen annealing from 29 to 40. Prior to metal deposition, the BST surface was cleaned by heating in the deposition chamber in low pressure oxygen atmosphere. In contrast, the samples deposited at $d = 7.5$ cm, 8.8 cm and 10 cm used in this study showed no improvement upon annealing. For this work smaller Pt top electrodes were structured using a photo resist. This processing

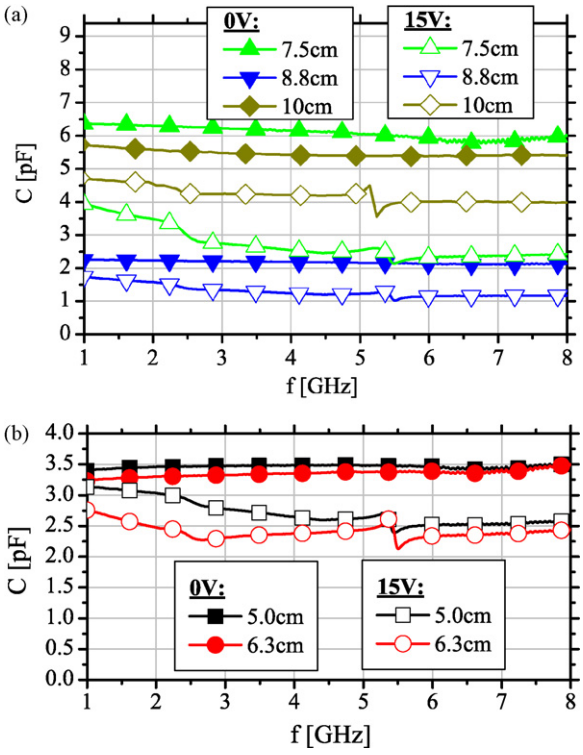

Fig. 10. Radio-frequency capacitance characteristics of the annealed BST varactors.

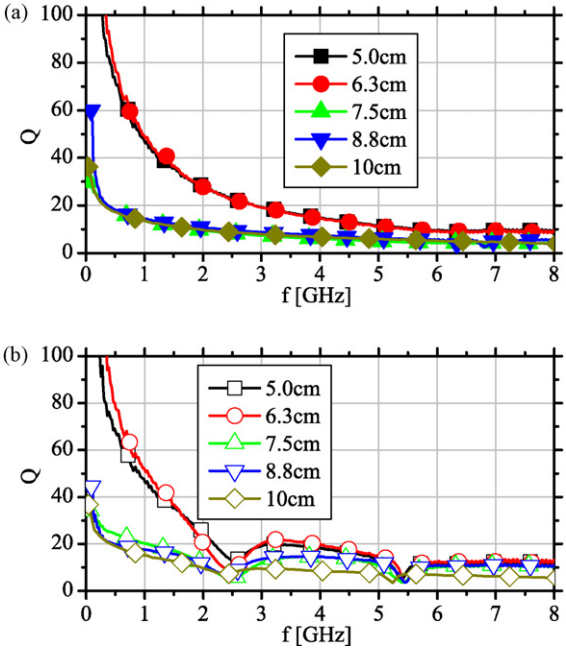

Fig. 11. Q-factor of the annealed BST varactors in (a) untuned and (b) tuned state at $U = +15$ V tuning voltage.

forbids a heating step in oxygen prior to annealing. Compared to silica or titania, the BST surface is prone to adsorption as measured with X-ray photoelectron spectroscopy.[39] Hence, the amount of adsorption is smaller on samples having high Ti excess. These adsorbates might protect the BST surface from defect formation during the Pt deposition which could lead to a higher Schottky barrier and more symmetric Q and I/V curves for the samples with a low Ti excess.

The difference in the amplitude of the leakage current can also be explained by the existence of the Ti excess in the BST thin films.[21,35] The amorphous TiO_{2-x} phase at the grain boundaries acts as a conductor and leads to a rise in the leakage currents of the BST films deposited at $d \leq 6.3$ cm. The increase of the leakage current is consistent with an increased doping level of the films, which is determined from the valence band maximum binding energies (see Section 2.2).

4. Thin film properties at microwave frequencies

The BST thin films are furthermore characterized at radio frequencies after the annealing step using an *Anritsu 37397C* vector-network analyzer. The measured capacitance value for 0 V and +15 V biasing are shown in Fig. 10(a) and (b) versus frequency.

The measured values of the untuned capacitances match quite well the 1 MHz measurement results, when the different varactor geometries are taken into account according to Eq. (2). The film deposited at 5 cm shows a relative permittivity of $\varepsilon_r(0) = 213$ at 1 MHz and of $\varepsilon_r(0) = 209$ at 2 GHz.

Applying a bias voltage of $U = 15$ V, acoustic resonances are raising up at 2.35 GHz and 5.2 GHz ($d = 10$ cm) by a switched-on piezoelectricity under bias. A model for acoustic resonances on such type of BST thin film varactors has been outlined in Ref. 13. The acoustic resonance is determined by the thickness of all stacked layers as well as the acoustic properties of the layers themselves. The frequency dependent impact of the acoustic resonances on the impedance of the capacitor can be modeled by using the equations of an acoustic transmission line model presented in Refs. 13 and 40 which enables in addition the characterization of the acoustic properties demonstrated in Ref. 41. The extracted acoustic impedance and velocity of the acoustic wave propagation for the presented BST thin films is presented in Ref. 41 resulting in a lowering of the acoustic impedance and a rising acoustic propagation velocity when the deposition distance is increased from 5 cm to 10 cm.

The microwave Q-factor measured at zero bias is shown in Fig. 11(a). Due to the thin Pt electrodes, additional frequency dependent losses in the metal electrodes arise at microwave frequencies and are responsible for the decrease of the Q-factor of the varactors with increasing frequency.[42] Therefore, Eq. (3) cannot be used to deduce directly the BST film properties from the microwave measurements. The losses induced by the electrodes in the microwave regime are the main factor limiting the Q-factor of the varactor.[8] They can be reduced by an increased metal thickness and/or a galvanic step for strengthening the electrodes with higher conductive metals.

In agreement with the 1 MHz measurements, the films with low Ti excess sputtered at $d \geq 7.5$ cm exhibit low Q-factors in the GHz range. The films deposited at 5 cm and 6.3 cm have higher Q-factors, where the value is limited by additional losses in the thin Pt electrodes.

The Q-factor for applied bias voltage is shown in Fig. 11(b). Caused by the acoustic resonances under bias the Q-factor decreases drastically at the resonance frequencies. Furthermore, the Q-factor for the varactors with $d \geq 7.5$ cm is increased by biasing comparable to the 1 MHz measurement.

5. Summary and conclusion

We have studied the structure, morphology, composition and electronic properties of BST thin films in dependence of the distance between target and substrate during magnetron sputter deposition using X-ray diffraction, electron microscopy, scanning force microscopy, Rutherford backscattering spectrometry and X-ray photoelectron spectroscopy. The results are linked to the electric and dielectric properties of varactors prepared with microstructured Pt electrodes. Dielectric characterization was carried out at 1 MHz and in the microwave frequency range up to 8 GHz, which is relevant for the application of this material in tunable capacitors.

The distance between target and substrate during sputter deposition was varied between 5 cm and 10 cm leading to a significant change in the Ti excess in the deposited films. A pronounced Ti excess is observed at lower distances, which results in a higher deposition rate. For distances $d > 7.5$ cm, stoichiometric films are obtained. Re-evaporation of Ba and Sr from the substrate surface during deposition due to slow oxide formation and high metal vapor pressure are suggested to be responsible for the Ti excess in the BST thin films.

The electric and dielectric properties also change drastically with sputter distance. At smaller distances, a reduced tunability coupled with a very low dielectric loss factor can be achieved whereas at larger distances a high tunability and increased dielectric loss factor are observed. The reduction of the tunability with increased Ti excess is inferior to the lowering of the dielectric loss factor resulting in an improved material quality factor $\eta = \tau/(\tan\delta)_{\max}$. In contrast to this improvement, the BST films having a high Ti excess show significantly larger leakage currents.

Annealing in oxygen leads to a strong decrease of leakage currents and a distinct increase of the Q-factors for the BST thin films with a high Ti excess. Annealing in oxygen also leads to symmetric behaviour with respect to the polarity of the tuning voltage. This is assigned to changes of the barrier height at the BST/Pt top electrode.

At microwave frequencies, the dielectric losses are dominated by losses in the metal electrodes and not by the BST thin film material. An improvement of capacitor layout and electrode thickness is required for further optimization. The losses are also affected by acoustic resonances of the layer stack, which are excited by the tuning voltage induced piezoelectricity of the BST film.

By varying the sputter distance, an appropriate material for different microwave applications can be designed. For applications where a high material quality factor is required the film deposited at 6.3 cm offers an outstanding η of 87 whereby the increased leakage current has to be taken into account. Furthermore, tunabilities higher than 70% at 67 V/μm with very low leakage currents can be achieved at 7.5 cm sputter distance. The structuring of Pt top electrodes on a closed BST thin film enables dielectric measurements in the lower GHz range in MIM topology without altering the BST thin film, e.g. by Ar dry etching. The presented dependence of the processing parameter and the related electric and dielectric properties can be used for a further optimization of varactors in the GHz range.

Acknowledgement

This work was supported by the German Research Foundation (DFG) within the DFG Research Training Group 1037 "Tunable integrated components in microwave technology and optics (TICMO)" and the European network of Excellence FAME.

References

1. Kozyrev, A., Ivanov, A., Keis, V., Khazov, M., Osadchy, V., Samoilova, T. *et al.*, Ferroelectric films: nonlinear properties and applications in microwave devices. In *Microwave Symposium Digest, 1998 IEEE MTT-S International*, 1998, pp. 985–988.
2. Kim, D., Je, S.-S., Kenney, J. and Marry, P., Design of ferroelectric phase shifters for minimum performance variation over temperature. In *Microwave Symposium Digest, 2004 IEEE MTT-S International, vol. 1*, 2004, pp. 257–260.
3. Tombak, A., Maria, J.-P., Ayguavives, F., Jin, Z., Stauf, G., Kingon, A. *et al.*, Voltage-controlled RF filters employing thin-film barium–strontium–titanate tunable capacitors. *IEEE Transactions on Microwave Theory and Techniques*, 2003, **51**(2), 462–467.
4. Papapolymerou, J., Lugo, C., Zhao, Z., Wang, X. and Hunt, A., A miniature low-loss slow-wave tunable ferroelectric bandpass filter from 11–14 GHz. In *Proceedings of the IEEE MTT-S International Microwave Symposium Digest*, 2006, pp. 556–559.
5. Scheele, P., Goelden, F., Giere, A., Mueller, S. and Jakoby, R., Continuously tunable impedance matching network using ferroelectric varactors. In *Microwave Symposium Digest, 2005 IEEE MTT-S International*, 2005, p. 4.
6. Schmidt, M., Lourandakis, E., Leidl, A., Seitz, S. and Weigel, R., A comparison of tunable ferroelectric Pi and T-matching networks. In *Proceedings of the 37th European Microwave Conference 2007*, 2007.
7. Tombak, A., A ferroelectric-capacitor-based tunable matching network for quad-band cellular power amplifiers. *IEEE Transactions on Microwave Theory and Techniques*, 2007, **55**(2), 370–375.
8. Marsan, E., Gauthier, J., Chaker, M. and Wu, K., Tunable microwave device: status and perspective. In *Proceedings of the 3rd International IEEE-NEWCAS Conference 2005*, 2005, pp. 279–282.
9. Tagantsev, A., Sherman, V., Astafiev, K., Venkatesh, J. and Setter, N., Ferroelectric materials for microwave tunable applications. *Journal of Electroceramics*, 2003, **11**, 5–66.
10. Akimov, I. A., Sirenko, A. A., Clark, A. M., Hao, J. H. and Xi, X. X., Electric-field-induced soft-mode hardening in SrTiO3 films. *Physical Review Letters*, 2000, **84**(20), 4625–4628.
11. Yamada, T., Shermana, V. O., Sua, D., Muralta, P., Tagantseva, A. K. and Setter, N., Growth process approaches for improved properties of tunable ferroelectric thin films. *Journal of the European Ceramic Society*, 2007, **27**, 3753–3758.
12. Setter, N., Damjanovic, D., Eng, L., Fox, G., Gevorgian, S., Hong, S. *et al.*, Ferroelectric thin films: review of materials, properties, and applications. *Journal of Applied Physics*, 2006, **100**, 051606.
13. Gevorgian, S., Vorobiev, A., Lewin, T., dc field and temperature dependent acoustic resonances in parallel-plate capacitors based on SrTiO3 and Ba0.25Sr0.75TiO3 films—experiment and modeling. *Journal of Applied Physics*, 2006, **99**, 124112.

14. Huang, S.-C., Chen, H.-M., Wu, S. C. and Lee, J. Y.-M., Time dependent dielectric breakdown of paraelectric barium–strontium–titanate thin film capacitors for memory device applications. *Journal of Applied Physics*, 1998, **84**(9), 5155–5157.
15. Lancaster, M. J., Powell, J. and Porch, A., Thin-film ferroelectric microwave devices. *Superconductor Science & Technology*, 1998, **11**(11), 1323–1334.
16. Vendik, O. G. and Zubko, S. P., Ferroelectric phase transition and maximum dielectric permittivity of displacement type ferroelectrics (Ba*x* Sr(1 − *x*)TiO3). *Applied Physics Letters*, 2000, **88**(9), 5343–5350.
17. Wang, X., Helmersson, U., Madsen, L. D., Ivanov, I. P., Munger, P., Rudner, S. *et al.*, Composition, structure, and dielectric tunability of epitaxial SrTiO3 thin films grown by radio frequency magnetron sputtering. *Journal of Vacuum Science & Technology A: Vacuum Surfaces and Films*, 1999, **17**(2), 564–570.
18. Im, J., Auciello, O., Baumann, P. K., Streiffer, S. K., Kaufman, D. Y. and Krauss, A. R., Composition-control of magnetron-sputter-deposited (BaxSr(1 − *x*))Ti(1 + *y*)O(3 + *z*) thin films for voltage tunable devices. *Applied Physics Letters*, 2000, **76**, 625–627.
19. Xu, J., Menesklou, W. and Ivers-Tiffee, E., Processing and properties of BST thin films for tunable microwave devices. *Journal of European Ceramic Society*, 2004, **24**, 1735–1739.
20. Kim, H. G., Preparation of ferroelectric thin-films for Si-based devices. *Integrated Ferroelectrics*, 1994, **4**, 371–381.
21. Yamamici, S., Yabuta, H., Sakuma, T. and Miyasaka, Y., (Ba + Sr)/Ti ratio dependence of the dielectric-properties for (Ba0.5Sr0.5)TiO3 thin-films prepared by ion-beam sputtering. *Applied Physics Letters*, 1994, **64**(13), 1644–1646.
22. Stemmer, S., Streiffer, S. K., Browning, N. D. and Kingon, A. I., Accommodation of nonstoichiometry in (100) fiber-textured (Ba(*x*)Sr(1 − *x*))Ti(1 + *y*)O(3 + *z*) thin films grown by chemical vapor deposition. *Applied Physics Letters*, 1999, **74**(17), 2432–2434.
23. Chu, W.-K., Mayer, J. W. and Nicolet, M. A., *Backscattering Spectrometry* (*1st edition*). Academic Press, New York, 1978.
24. Moulder, J., Stickle, W., Sobol, P. and Bomben, K., *Handbook of X-ray Photoelectron Spectroscopy*. Perkin-Elmer Corp, Eden Prairie, MN, USA, 1992.
25. Szot, K., Speier, W., Breuer, U., Meyer, R., Szade, J. and Waser, R., Formation of micro-crystals on the (1 0 0) surface of SrTiO3 at elevated temperatures. *Surface Science*, 2000, **460**(1–3), 112–128.
26. Meyer, R., Waser, R., Helmbold, J. and Borchardt, G., Observation of vacancy defect migration in the cation sublattice of complex oxides by O18 tracer experiments. *Physical Review Letters*, 2003, **90**(10), 105901.
27. Chapman, B., *Glow Discharge Processes: Sputtering and Plasma Etching* (*1st edition*). John Wiley & Sons Inc., 1980.
28. Ohring, M., *Materials Science of Thin Films. Deposition and Structure* (*2nd edition*). Academic Press, 2001.
29. Klein, A. and Saeuberlich, F., *Surfaces and Interfaces of Sputter-Deposited ZnO Films*. Springer-Verlag, Berlin, 2008.
30. Schafranek, R., Payan, S., Maglione, M. and Klein, A., Barrier height at (Ba,Sr)TiO3/Pt interfaces studied by photoemission. *Physical Review B*, 2008, **77**(19), 195310.
31. Kraut, E. A., Grant, R. W., Waldrop, J. R. and Kowalczyk, S. P., Semiconductor core-level to valence-band maximum binding-energy differences: precise determination by X-ray photoelectron spectroscopy. *Physical Review B*, 1983, **28**(4), 1965.
32. Chase, D., Chen, L.-Y. and York, R., Modeling the capacitive nonlinearity in thin-film BST varactors. *IEEE Transactions on Microwave Theory and Techniques*, 2005, **53**(10), 3215–3220.
33. Maria, J.-P., Boyette, B., Kingon, A., Ragalia, C. and Stauf, G., Low loss tungsten-based electrode technology for microwave frequency BST varactors. *Journal of Electroceramics*, 2005, **14**, 75–81.
34. Baniecki, J. D., Laibowitz, R. B., Shaw, T. M., Saenger, K. L., Duncombe, P. R., Cabral, C., Kotecki, D. E., Shen, H., Lian, J. and Ma, Q. Y., Effects of annealing conditions on charge loss mechanisms in MOCVD Ba0.7Sr0.3TiO3 thin film capacitors. *Journal of the European Ceramic Society*, 1999, **19**(6–7), 1457–1461.
35. Stemmer, S., Streiffer, S., Browning, N., Basceri, C. and Kingon, A., Grain boundaries in barium strontium titanate thin films: structure, chemistry and influence on electronic properties. *Interface Science*, 2000, **8**, 209–221.
36. Muller, K. H., Role of incident kinetic-energy of adatoms in thin-film growth. *Surface Science*, 1987, **184**(1–2), L375–L382.
37. Wang, D. Y., Electric and dielectric-properties of barium–titanate schottky-barrier diodes. *Journal of the American Ceramic Society*, 1994, **77**(4), 897–910.
38. Cramer, N., Mahmud, A. and Kalkur, T. S., Effect of annealing on leakage current in Ba0.5Sr0.5TiO3 and Ba0.96Ca0.04Ti0.84Zr0.16O3 thin films with Pt electrodes. *Applied Physics Letters*, 2005, **87**(3), 32903.
39. Schafranek, R., et al., submitted for publication.
40. Turalchuk, P., Vendik, I., Vendik, O. and Berge, J., Modelling of tuneable acoustic resonators based on BSTO films with induced piezoelectric effect. In *Proceedings of the 37th European Microwave Conference*, 2007.
41. Giere, A., Schafranek, R., Zheng, Y., Maune, H., Sazegar, M., Jakoby, R. and Klein, A., Characterization of acoustic effects in ferroelectric thin-films for microwave components. *FREQUENZ*, 2008, **3–4**, 52–56.
42. Dube, D. C., Baborowski, J., Muralt, P. and Setter, N., The effect of bottom electrode on the performance of thin film based capacitors in the gigahertz region. *Applied Physics Letters*, 1999, **74**, 3546–3548.